Spectral shaping to improve the point spread function in optical coherence tomography

A. Ceyhun Akcay and Jannick P. Rolland

School of Optics, Center for Research and Education in Optics and Lasers, University of Central Florida, 4000 Central Florida Boulevard, Orlando, Florida 32816-2700

Jason M. Eichenholz

Newport Corporation, 1791 Deere Avenue, Irvine, California 92606

Received July 14, 2003

We demonstrate inhibition of the sidelobes of the axial point spread function in optical coherence tomography by shaping the power spectrum of the light source with a remaining power of 4.54 mW. A broadband amplified spontaneous emission source radiating at 1565 ± 40 nm is employed in a free-space optical coherence tomography system. The axial point spread functions before and after optical spectral shaping are presented. Results show that spectral shaping of the source can inhibit sidelobes of the point spread function up to 12.9 dB, with an associated small increase of 2.2 dB in noise floor in the far field. The effect of spectral shaping on axial resolution is demonstrated according to three metrics. Image quality improvement is also illustrated with optical coherence tomography images of an onion before and after spectral shaping.

OCIS codes: 170.4500, 110.4500, 350.5730, 120.3180.

Optical coherence tomography[1,2] (OCT) is an interferometric biomedical imaging technique for obtaining high-resolution cross-sectional images of highly scattering tissue. A near-infrared light source that has a broad spectral bandwidth and therefore a short coherence length illuminates the sample through an interferometer. The temporal coherence property of the light source or power spectrum governs the axial point spread function (PSF) of the imaging system,[3,4] and thus the axial resolution. Axial resolution may be quantified through common metrics such as the full width at half-maximum (FHWM), the absolute square integral (ASI),[3,5] and the root-mean-square (rms) width[6] of the axial PSF. In OCT, light sources with smooth and rather symmetrical power spectra are preferred. Specifically, irregularities in the shape of the power spectrum such as spectral dips lead to sidelobes in the axial PSF that cause ghost images and mask weak axial reflections located near a strong reflection.[3,4,7,8] Real broadband light sources, however, often present spectral dips in their power spectra, especially as the source spectra become broader. In this Letter we demonstrate sidelobe inhibition by optical shaping of the source power spectrum without significantly increasing the far-field noise floor of the axial PSF. Furthermore, axial resolution before and after spectral shaping is presented according to the FWHM, the ASI, and rms width resolution metrics. Finally, OCT images before and after shaping are presented.

Inhibition of the sidelobes of spatial PSFs in optical imaging has been one of the major areas of study in imaging. For example, Crowe *et al.*[9] proposed a nonlinear digital operator to be applied in postprocessing to suppress the sidelobe effect of the spatial PSF on images obtained through a square aperture. Similarly, digital signal processing and optimization algorithms on the acquired interferometric signal were previously employed in OCT to increase resolution or to minimize the effect of the PSF sidelobes when the source had either a power spectrum departing from a Gaussian or several sources combined to generate a source with a larger spectral bandwidth. Bashkansky *et al.*[10] showed how a simple deconvolution can lead to an equivalent reshaping of the spectrum structure of the source, resulting in an increase in axial resolution. However, this method leads to a significant increase of the noise floor. Tripathi *et al.*[7] later proposed reducing the sidelobes in the axial PSF by applying a correction curve to the measured interferometric signal. They reported reduction of sidelobes, with a lower increase in noise floor. Zhang *et al.*[8] demonstrated an optimization algorithm with which to select the wavelengths and coherence lengths of several LEDs that were combined to yield an axial PSF with a shorter coherence length and reduced sidelobes compared with an arbitrary combination of sources. However, all the methods described above are based on post-data-acquisition signal-processing techniques. In this Letter we present experimental results demonstrating inhibition of sidelobes of the axial PSF in OCT by optical spectral shaping of the source power spectrum before data acquisition. This research is motivated by real-time *in vivo* imaging and by the hypothesis that correcting the power spectrum before data acquisition may be more useful for practical use than as a postprocessing correction.

The ac part of the interferometric signal in a free-space Michelson interferometer with an optical path length difference between the interferometer arms given by Δz is proportional to

$$I(\Delta z) \propto \mathrm{Re} \int E_R(t) E_S{}^*\left(t - \frac{2\Delta z}{c}\right) \mathrm{d}t , \qquad (1)$$

0146-9592/03/201921-03$15.00/0

where $E_R(t)$ and $E_S(t)$ are the detected optical fields from the reference and the sample arms, respectively, Re denotes the real part, and c is the speed of light. The interferometric signal in expression (1) is the self-coherence function if the optical fields in the two arms are equal. Hence, the inverse Fourier transform of the power spectrum of the light source is equal to expression (1), as stated by the Wiener–Khintchine theorem.[11] The envelope of the self-coherence function defines the axial PSF of the imaging system and can be given by

$$\mathrm{PSF}(\Delta z) \propto \left| \int S(\lambda) \exp\left[i \frac{2\pi}{\overline{\lambda}^2} (\lambda - \overline{\lambda}) 2\Delta z \right] \mathrm{d}\lambda \right|, \quad (2)$$

where $S(\lambda)$ is the power spectrum of the source and $\overline{\lambda}$ is its mean wavelength.

In Ref. 3, Akcay *et al.* discussed the effect of the shape of the source power spectrum on the interferometric signal and simulated the axial PSFs for a real superluminescent diode and virtual ideal sources with specific spectral characteristics. In this Letter we propose a new use of a programmable spectral processor (PSP; Newport OSP-9100). For what is believed to be the first time, this component is shown to be applicable to optical shaping of the power spectrum of a broadband source for OCT. This processor is based on the Texas Instrument DLP micromirror technology.[12] Light enters the PSP via a single-mode fiber, is dispersed across the micromirror array by a diffraction grating, and is then reimaged into the exit fiber via the grating. The hundreds of thousands of micromirrors in the array act as a spatial light modulator, selectively reflecting portions of the spectrum into the exit fiber while simultaneously eliminating or reducing portions of the original spectral components, such as spectral dips, that are not desirable.

A free-space Michelson interferometer, depicted in Fig. 1, was implemented with a balanced photoreceiver (Nirvana 2017-M) to measure the axial PSF before and after optical spectral shaping. A broadband amplified spontaneous emission source (Newport BBS-430) emitting at 1565 ± 40 nm was employed in the experiments. The PSP was connected to the amplified spontaneous emission source through a single-mode fiber patch cord. The optical power at the output of the PSP was 7.72 mW, and it passed through the PSP without any shaping. A fiber pigtailed collimator delivered the optical power from the output of the PSP to the interferometer. Axial scanning was performed at a speed of 1 mm/s with a translational stage.

Figure 2 shows the measured power spectrum of the amplified spontaneous emission source, $S(\lambda)$. A Gaussian power spectrum, $S_g(\lambda)$ that could fit within the measured power spectrum of the source was generated digitally with MATLAB software. A transmission curve, $\Delta(\lambda)$, was computed as the ratio of the generated $S_g(\lambda)$ and the original $S(\lambda)$ power spectra when $S(\lambda)$ was larger than or equal to $S_g(\lambda)$. Otherwise, $\Delta(\lambda)$ was assigned a value of zero, since the PSP cannot amplify optical power at any wavelength. $\Delta(\lambda)$ was converted to decibel scale, and each value was rounded to a single decimal place, since the amplitude resolution of the PSP was 0.1 dB. This transmission function was sent to the PSP via a general purpose interface bus. The final power spectrum shaped by the PSP is shown in Fig. 2 by the dashed curve. The total power loss after spectrum shaping was −2.3 dB, corresponding to 4.54 mW of output power. Following the same procedure, we also shaped the source power spectrum into a power spectrum that had a smoother transition from the central portion of the power spectrum toward its tails, as shown by the dotted curve in Fig. 2. For this case, the total power loss was −3.4 dB, corresponding to 3.53 mW of output power.

Figure 3 shows the axial PSFs corresponding to the original spectrum as well as the first shaped spectrum (i.e., the dashed curve in Fig. 2). With this shaping operation, up to 12.9-dB suppression in the sidelobes of the axial PSF was obtained, as shown in Fig. 3. The noise floor of the axial PSF in the far-field increased by only 2.2 dB. Similarly, with the second spectrum-shaping operation (i.e., the dotted curve in Fig. 2), up to 7.6-dB suppression in the sidelobes of the axial PSF was obtained. The increase of the axial PSF in the far field in this case was as small as 1.8 dB. In Table 1, the associated changes in the FWHM, the ASI, and the rms width of the axial PSFs of the original spectrum as well as those of the two shaped spectra are reported. Although the FWHM metric predicts a small loss in resolution, the two other metrics indicate either an increase or

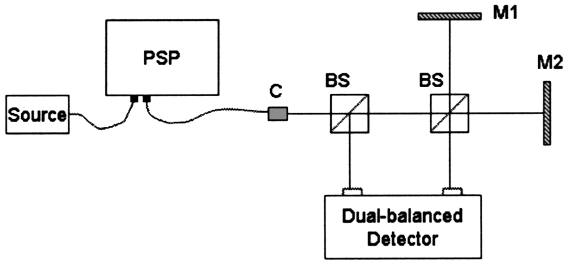

Fig. 1. Schematic of the experimental setup used for axial PSF measurements: C, collimator; BSs, beam splitters; M1, M2, mirrors.

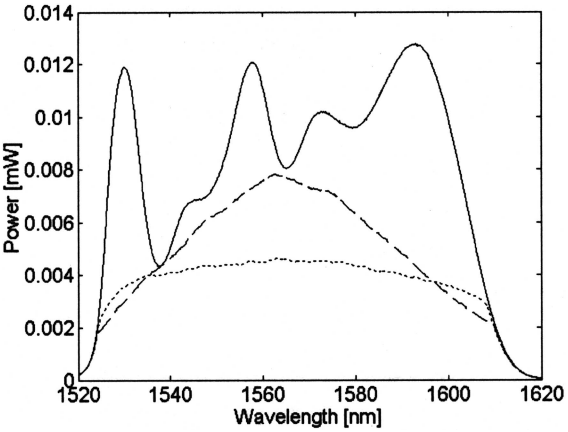

Fig. 2. Power spectra. Solid curve, original power spectrum of the source; dashed curve, power spectrum after the first shaping operation; dotted curve, power spectrum after the second shaping operation.

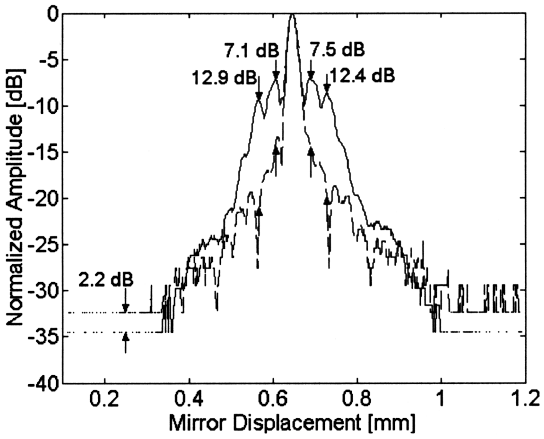

Fig. 3. Axial PSFs: solid curve, original source power spectrum; dashed curve, power spectrum presented by the dashed curve in Fig. 2.

Table 1. Axial Resolution of the Differently Shaped Power Spectra Computed According to the Three Metrics Illustrated in Fig. 2

Axial PSF	FWHM (μm)	ASI (μm)	rms Width (μm)
Solid curve	22.3	19.9	19.74
Dashed curve	24.9	19.1	20.05
Dotted curve	24	18.6	20.03

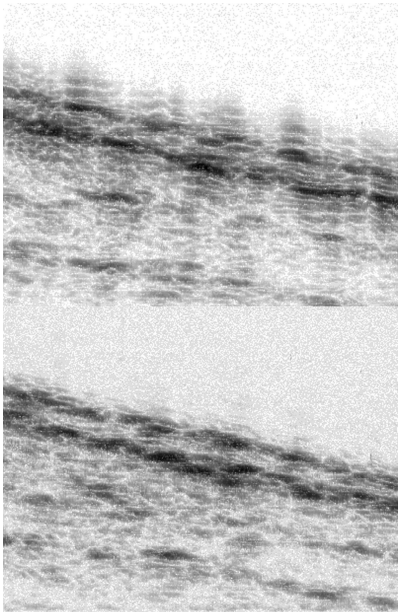

Fig. 4. Images of onion (top) before and (bottom) after spectral shaping. The image sizes are 1 mm $\times$ 1 mm.

an insignificant change in axial resolution, pointing to the need to further investigate experimentally the applied significance of the various resolution metrics.

Figure 4 shows from top to bottom typical images formed by the original spectrum and by a shaped spectrum. These data are raw data with no averaging to reduce background noise and no image processing applied. Both images are 400 $\times$ 400 pixels and represent a 1 mm $\times$ 1 mm portion of an onion. Throughout the unshaped spectrum image, spurious structures are visible as a consequence of the sidelobes of the PSF. The spectrally shaped image clearly shows sidelobe suppression and a higher definition of the layers in the image.

In conclusion, we have investigated the effect of optical spectral shaping of an OCT light source on the axial PSF of the system. The programmable spectral processor made it possible to shape the source power spectrum and inhibit the sidelobes of the axial PSF for two different spectral shapes that were smoother than the original spectrum. Optical spectral shaping is a real-time process and allows hardware optimization for imaging.

We thank Eric Clarkson for suggesting the rms-width measure of the PSF as a common metric of resolution and for stimulating discussion about this work. We also thank Jim Sirkis and Jerrin Russell of Cidra Corp. and Hector Lara of Newport Corp. for their assistance with the PSP. This work was supported by the National Science Foundation/ Information Technology Research IIS-00-82016, the U.S. Army Simulation, Training, and Instrumentation Command, and the Newport Corporation. J. P. Rolland's e-mail address is jannick@odalab.ucf.edu.

References

1. D. Huang, E. A. Swanson, C. P. Lin, J. S. Schuman, W. G. Stinson, W. Chang, M. R. Hee, T. Flotte, K. Gregory, C. A. Puliafito, and J. G. Fujimoto, Science **254,** 1178 (1991).
2. J. M. Schmitt, IEEE J. Sel. Top. Quantum Electron. **5,** 1205 (1999).
3. C. Akcay, P. Parrein, and J. P. Rolland, Appl. Opt. **41,** 5256 (2002).
4. B. E. Bouma and G. J. Tearney, in *Handbook of Optical Coherence Tomography*, B. E. Bouma and G. J. Tearney, eds. (Marcel Dekker, New York, 2002), pp. 67–97.
5. L. Mandel and E. Wolf, *Optical Coherence and Quantum Optics* (Cambridge U. Press, New York, 1995), p. 179.
6. E. Sorokin, G. Tempea, and T. Brabec, J. Opt. Soc. Am. B **17,** 146 (2000).
7. R. Tripathi, N. Nassif, J. S. Nelson, B. H. Park, and J. F. de Boer, Opt. Lett. **27,** 406 (2002).
8. Y. Zhang, M. Sato, and N. Tanno, Opt. Lett. **26,** 205 (2001).
9. D. G. Crowe, J. Shamir, and T. W. Ryan, Appl. Opt. **32,** 179 (1993).
10. M. Bashkansky, M. D. Duncan, and J. Reintjes, Appl. Opt. **37,** 8137 (1998).
11. J. W. Goodman, *Statistical Optics* (Wiley, New York, 1985), pp. 73–76.
12. W. Duncan, B. Lee, P. Rancuret, B. Sawyers, W. Stalcup, L. Endsley, and D. Powell, Proc. SPIE **4983,** 297 (2003).